9-2019

A geomorphic enthalpy method: Description and application to the evolution of fluvial-deltas under sea-level cycles

William Anderson
Montclair State University

Jorge Lorenzo Trueba
Montclair State University, lorenzotruej@mail.montclair.edu

Vaughan Voller
University of Minnesota

Manuscript accepted in Computer & Geosciences in April 2019

A geomorphic enthalpy method: Description and application to the evolution of fluvial-deltas under sea-level cycles

William Anderson[1], Jorge Lorenzo-Trueba[2*], Vaughan Voller[3]

[1] Department of Mathematical Sciences, Montclair State University, Montclair, USA

[2] Department of Earth and Environmental Studies, Montclair State University, Montclair, USA

[3] Department of Civil Engineering, University of Minnesota, Minneapolis, USA

* Corresponding author: Jorge Lorenzo-Trueba. Email address: lorenzotruej@montclair.edu

* Corresponding author address: CELS 302, 1 Normal Ave, Montclair State University, Montclair, NJ 07043.

Link to the code: https://github.com/JorgeMSU/1D-enthalpy-method

Highlights:

- Enthalpy-like solution to study fluvio-deltaic dynamics under sea-level variations.
- Model produces stratigraphic profiles under a wide range of sea-level curves.
- Time lags in system response can lead to river incision during the sea-level rise.

Authorship statement: WA and JLT developed the theory and performed the computations with input from VV. JLT and WA wrote the manuscript with input from VV. JLT designed and directed the project.

Abstract

Fluvial deltas are composites of two primary sedimentary environments: a depositional fluvial region and an offshore region. The fluvial region is defined by two geomorphic moving boundaries: an alluvial-bedrock transition (ABT), which separates the sediment prism from the non-erodible bedrock basement, and the shoreline (SH), where the delta meets the ocean. The trajectories of these boundaries in time and space define the evolution of the shape of the sedimentary prism, and are often used as stratigraphic indicators, particularly in seismic studies, of changes in relative sea level and the identification of stratigraphic sequences. In order to better understand the relative role of sea-level variations, sediment supply, and basin geometry on the evolution of the ABT and SH, we develop a forward stratigraphic model that accounts for curvature changes of the fluvial surface and treats the SH and ABT as moving boundaries (i.e., internal boundaries that are not known a priori and their location must be calculated as part of the solution to the overall problem). This forward model extends a numerical technique from heat transfer (i.e., enthalpy method), previously applied to the evolution of sedimentary basins, to account for sea-level variations, including eustatic sea-level cycles. In general, model results demonstrate the importance of the dynamics of the fluvial surface on the system response under a large range of input parameter values. Specifically, model results suggest that time lags in the ABT response during sea-level cycles can result in geologically long-lived river incision in the upper and mid portions of the fluvial surface during sea-level rise. These results suggest that the relationship between the coastal onlap configuration of strata and relative changes in sea level is complex, and therefore not necessarily a good indicator of contemporaneous sea-level changes.

Keywords: Enthalpy method, Fluvial deltas, sea-level cycles, Alluvial-basement transition, Shoreline, river incision

1. Introduction

Fluvial deltas are composites of several basic environments, including a depositional fluvial region and a subaqueous offshore region, that generally resemble a triangular prism superimposed upon a relatively planar basement profile (Figure 1a; Chavarrías et al., 2018; Lorenzo-Trueba et al., 2009; Paola, 2000; Posamentier et al., 1992; Swenson et al., 2005). This triangular sedimentary prism presents three geomorphic boundaries or vertices: the alluvial-bedrock transition (ABT), which separates the bedrock (or basement) from the depositional fluvial region, the shoreline (SH), which separates the fluvial region from the subaqueous depositional region, and the delta toe where the subaqueous sediment wedge intersects with the basement. Changes in the length of the depositional fluvial domain occur via transgression (i.e., SH landwards migration), regression (i.e., SH seawards migration), coastal onlap (i.e., ABT landwards migration), and coastal offlap (i.e., ABT seawards migration) (see Figure 1). These changes are in general a function of the sediment supply to the sedimentary prism, the efficacy of the sediment transport and deposition along the fluvial surface, and relative sea-level variations (i.e., the combination of eustatic sea level changes and subsidence). For instance, if sediment supply is high relative to both the length of the fluvial surface and the accommodation created by sea-level rise, the results is SH regression and coastal onlap, which causes an overall lengthening of the sedimentary prism, as well as an increase in elevation (i.e., river aggradation) of the fluvial surface (Figure 1b). A combination of relative sea-level fall with low sediment supply, however, typically results in regression, coastal offlap, and a decrease in elevation (i.e., river degradation) of the fluvial surface (Figure 1c). Additionally, Muto and Steel (2002) found that a low sediment supply relative to the length of the fluvial surface and the rate of relative sea-level rise can lead to a break in the triangular geometry of the sedimentary prism as the system transgresses (Figure 1d).

Cycles of SH transgression/regression and coastal onlap/offlap in the sedimentary record (Figure 1) can potentially allow for reconstruction of a basin's history of sediment supply and paleo–sea level (Henriksen et al., 2009; Törnqvist et al., 2006). To tackle this inverse problem, the migration of the internal boundaries that describe the evolution of the system (e.g., ABT, SH) have to be computed as a part of the solution to the overall geological problem (Lorenzo-Trueba et al., 2013, 2009; Lorenzo-Trueba and Voller, 2010; Marr et al., 2000; Swenson et al., 2000). Analogous to the migration of the ice/water front in a one phase Stefan melting problem (Crank, 1984), Swenson et al. (2000) applied this framework to the migration of the SH in sedimentary basins. In particular, these authors used an analogy between heat and sediment diffusive transport to describe the movement of the SH under varying conditions of sediment supply and relative sea level. Follow-up work by Voller et al. (2004) found that in the particular case of constant sediment supply and a fixed sea level, the problem presented by Swenson et al. (2000) allows for a closed-form analytical solution. Based on Voller et al. (2004), Capart et al. (2007), and Lai and Capart (2007) developed analytical solutions in which the ABT and the SH were treated as independent moving boundaries. Lorenzo-Trueba et al. (2009) expanded on this work by developing an analytical solution able to track both the ABT and the SH under conditions of constant sediment supply and fixed sea-level. Lorenzo-Trueba et al. (2009) also validated this solution against flume experiments under a range of system parameters. In addition to studying the kinematics of ocean shoreline deltas, similar models and solution methodologies along the lines of those noted above, have also been applied in studies of lake deltas and morphology, e.g., (Capart et al., 2010).

Although simplified solutions can increase the clarity and insights the model facilitates, moving boundary problems only have analytical solutions in a limited range of scenarios. In order to study more general cases, different numerical methods have been developed for the dual ABT and SH moving boundary problem (Lorenzo-Trueba and Voller, 2010; Parker et al., 2008; Voller et al., 2006). Parker et al. (2008) developed a deforming grid method, based on a Landau front-fixing approach, able to track both the ABT and the SH under constant sea-level rise in a one-dimensional setting. A drawback of the deforming grid method, however, is that the extension to two-dimensions is far from straightforward. Voller et al. (2006) developed a solution based on the enthalpy method, able to operate on a fixed grid under constant sea level, and focused on the dynamics of the SH. Lorenzo-Trueba and Voller (2010) extended this numerical solution to account for the migration of both the ABT and SH. Despite these recent developments, however, to date all numerical solutions had been restricted to either a fixed sea level or constant sea-level rise scenarios. The only attempt to solve the problem under sea-level cycles was by Lorenzo-Trueba et al. (2013), who developed an integral approximation of the Exner equation assuming a quadratic fluvial surface profile. This solution, however, is not able to account for full cycles of transgression and regression (only cases where transgression follows regression). Thus, our first goal is to extend the enthalpy-like numerical solution from Lorenzo-Trueba and Voller (2010) to account for sea-level cycles, as well as cycles of SH transgression/regression. Second, we investigate potential modes of coastal behavior under sea-level cycles and a wide range of system parameters.

2. The Dual Moving Boundary Problem

2.1 Equations

We model fluvio-deltaic evolution in cross-section as described in Figure 2a. As opposed to previous modeling efforts that account for different shoreface morphologies (Lai and Capart, 2007; Swenson et al., 2005), temporal changes in sediment supply (An et al., 2017), or breaks in the basement slope (Lai et al., 2017), we assume a linear basement slope β, a linear foreset slope ψ, and a steady sediment supply q_0. We adopt this idealized cross-shore geometry to simplify the calculations and focus on the role of the fluvial surface dynamics on the response of the system. Given such cross-shore geometry (Figure 2), the evolution of the fluvio-deltaic system can be described in terms of the locations of the ABT ($x = r(t)$), the SH ($x = s(t)$), and the delta toe ($x = w(t)$). In the absence of differential subsidence, we can describe changes in the elevation h at any location of the fluvial surface with respect to current sea level (Figure 2a) as the divergence of the sediment flux q (Paola and Voller, 2005),

$$\frac{\partial h}{\partial t} = -\frac{\partial q}{\partial x}, \quad r(t) \leq x \leq s(t) \tag{1}$$

where x is positive in the seaward direction, and $x=0$ is located at the intersection between the initial sea level and the basement.

Following numerous efforts, which include both numerical modeling and laboratory experiments (Paola et al., 1992; Ribberink and van der Sande, 1985; Fagherazzi and Overeem, 2007; Parker and Muto, 2003; Postma et al., 2008; Swenson et al., 2000; Swenson and Muto, 2007), we assume that q is primarily controlled by the fluvial slope. In particular, for simplicity we assume that q is linearly related to the fluvial slope as follows (Paola et al., 1992; Lorenzo-Trueba et al., 2013; Lorenzo-Trueba and Voller, 2010; Marr et al., 2000; Swenson et al., 2000; Swenson and Muto, 2007)

$$q(x) = -\nu \frac{\partial h}{\partial x} \quad (2)$$

where ν is the 'fluvial diffusivity', which can be calculated as a function of water discharge and grain size characteristics (Paola, 2000).

The combination of equations (1) and (2) leads to the so-called linear diffusion equation, which generally requires two boundary conditions and an initial condition to be solved. In this case, however, the locations of the ABT and the SH (i.e., *r* and *s*) are unknown a priori and need to be solved as part of the solution. Consequently, the problem requires four boundary conditions instead of just two. The first condition matches the fluvial surface elevation at the ABT to the basement elevation:

$$h|_{x=r} = -\beta r \quad (3a)$$

The second condition implies that the elevation of the fluvial surface at the SH is equal to sea level:

$$h|_{x=s} = Z \quad (3b)$$

where Z is the sea level. The third condition imposes a given sediment input q_0 at the ABT:

$$-\nu \frac{\partial h}{\partial x}\Big|_{x=r} = q_0 \quad (3c)$$

The fourth condition in general relates the sediment flux that reaches the SH with the rate of migration of the foreset toe, which is defined as $dw/dt = ds/dt + 1/\psi \cdot dZ/dt$ (Swenson et al., 2000). In the particular case in which the shoreface toe only migrates seawards (i.e., $dw/dt > 0$), the system maintains the wedge geometry depicted in Figure 1, and we can define the basin depth as $D(x,t) = \psi/(\psi - \beta) \cdot (s\beta + Z)$ (Lorenzo-Trueba et al., 2013). For simplicity, however, given that the foreset slope ψ is generally orders of magnitude larger than any other slope in the system, including the basement slope β, we assume $\psi/(\psi - \beta) \sim 1$ (Edmonds et al., 2011; Lorenzo-Trueba et al., 2013, 2009; Lorenzo-Trueba and Voller, 2010; Swenson and Muto, 2007). This assumption implies that a shift from regression to transgression coincides with the abandonment of the subaqueous foreset, which means that the SH and the delta toe always migrate in the same direction (i.e., $dw/dt = ds/dt$). In this scenario, the fourth boundary relates the sediment flux that reaches the SH with the rate of migration of the SH and the ocean depth as follows:

$$-v\left.\frac{\partial h}{\partial x}\right|_{x=s} = \begin{cases} D(x,t)\frac{ds}{dt}, & \frac{ds}{dt} > 0 \\ 0, & \frac{ds}{dt} \leq 0 \end{cases} \tag{3d}$$

When the SH migrates seawards (i.e., $ds/dt > 0$) beyond past SH locations, the system maintains the wedge geometry and the basin depth reduces to $D(x,t) = s\beta + Z$. In contrast, when all sediments deposit on the fluvial surface before reaching the SH, the SH sediment flux is equal to zero and the SH migrates landwards (i.e., $ds/dt \leq 0$). Under this condition, the SH detaches from the subaqueous foreset (Figure 2b), a condition previously defined as ‘autobreak’ (Muto and Steel, 2002). Additionally, in some instances the SH migrates seaward (i.e., $ds/dt >$

0) over subaqueous deposits left during autobreak, in which case $D(x, t)$ corresponds to the ocean depth of these offshore deposits (Figure 2c).

Under these conditions, with equations (1-3) and a given initial geometry: $s(0) = r(0) = 0$, we can fully describe the dynamics of the fluvial surface under sea-level changes, including cycles of regression and transgression (Figure 2).

2.2 A dimensionless form

In this section, we reduce the number of controlling parameters to a minimum by rewriting the governing equations (1-3) in dimensionless form. The scaling used towards this end is as follows

$$x^d = \frac{x}{l}, \;\; t^d = \frac{t}{\tau}, \;\; s^d = \frac{s}{l}, \;\; r^d = \frac{r}{l}, \;\; Z^d = \frac{Z}{l\beta}, \;\; h^d = \frac{h}{l\beta}, \;\; D^d = \frac{D}{l\beta}, \;\; q^d = \frac{q\tau}{l^2\beta} \tag{4}$$

where l is the horizontal scale (e.g., a characteristic delta length), $l\beta$ is the vertical scale, and $\tau = l^2/\nu$ is an 'equilibrium timescale' defined by Paola et al. (1992). From the scaling in (4), we obtain one dimensionless group: the ratio of the fluvial to the bedrock slope at the ABT

$$R_{ab} = -\frac{1}{\beta}\frac{\partial h}{\partial x}\bigg|_{x=r} = \frac{q_0}{\beta \nu} \tag{5}$$

which is physically constrained within the range $0 < R_{ab} < 1$.

Dropping the d superscript for convenience of notation, the dimensionless versions of equations (1) to (3) become:

$$\frac{\partial h}{\partial t} = \frac{\partial^2 h}{\partial x^2}, \quad r(t) \le x \le s(t) \tag{6}$$

with conditions

$$h|_{x=r} = -r \tag{7a}$$

$$h|_{x=s} = Z \tag{7b}$$

$$-\frac{\partial h}{\partial x}\bigg|_{x=r} = R_{ab} \tag{7c}$$

$$-\frac{\partial h}{\partial x}\bigg|_{x=s} = \begin{cases} D(x,t)\frac{ds}{dt}, & \frac{ds}{dt} > 0 \\ 0, & \frac{ds}{dt} \leq 0 \end{cases}. \tag{7d}$$

The initial conditions are:

$$s(t=0) = r(t=0) = 0. \tag{8}$$

In the particular case in which the SH only migrates seawards (i.e., $ds/dt > 0$), the system maintains the wedge geometry depicted in Figures 1a and 2a, and we can define the basin depth as $D(x,t) = s + Z$ (Lorenzo-Trueba et al., 2013). Under this special case, equations (6) – (8) admit close form analytical solutions, which are described in section 4. In general, however, these equations require a numerical solution.

3. The Geomorphic Enthalpy Method

In this section, we develop a numerical solution able to operate in cases where the closed form solutions do not hold. Moreover, the objective of this section is to present a fixed grid enthalpy-like method that solves the problem numerically without the need of tracking the ABT and the SH as part of the solution (Voller et al. 2006; Lorenzo-Trueba and Voller 2010). With this objective in mind, we define the enthalpy function $H(x,t)$, which in our case represents the sediment prism thickness (Figure 3), as follows:

$$H(x,t) = h(x,t) + Z(t) - E(x) \tag{9}$$

where $E(x)$ denotes the basement elevation, i.e., $E(x) = -x$. Inverting (9), we can describe the elevation respect to current sea level (Figure 2a) anywhere in the domain as follows

$$h = \max(H + E - Z, 0)\ . \tag{10}$$

As defined by equation (10), h is always greater than zero landward of the SH, and zero seawards of the SH (Figure 3). Consequently, sediment fluxes as described in equation (2) are zero beyond the SH, which implies that the subaqueous portion of the fluvial-delta maintains its sediment thickness and hence its shape. Although we believe this is a reasonable assumption to first order, future versions of the model will investigate the effect of waves and tides on the transport of sediments in the subaqueous portion.

Equations (9) and (10) are fully consistent with the original enthalpy formulation introduced by Crank (1984). However, as previously noted by Voller et al. (2006) and Lorenzo-Trueba and Voller (2010), in this case the term representing the latent heat $L(x,t) = Z(t) - E(x)$ can be a function of space and time. Using equations (9) and (10), we can then describe the problem using the same sediment balance equation for the full solution space, i.e.,

$$\frac{\partial H}{\partial t} = -\frac{\partial q}{\partial x}, \quad -\infty \leq x \leq \infty \tag{11}$$

where q is the sediment flux described in equation (2). At the upstream limit of the domain, the sediment flux is always equal to the sediment input, which in dimensionless numbers is equal to R_{ab}, i.e., $\lim_{x \to -\infty} q = R_{ab}$. At the downstream limit of the domain, the elevation above sea level is always equal to zero, i.e., $\lim_{x \to \infty} h = 0$. Equation (11) also requires initial conditions to be solved, which we define as follows

$$H(x,0) = 0 \tag{12a}$$

$$h(x,0) = \begin{cases} -x, & x < 0 \\ 0, & x \geq 0 \end{cases}. \tag{12b}$$

We develop a numerical solution for equations (9) to (12) based on a uniform grid size Δx and time step size Δt. We set the origin point $x = 0$, where the ABT and SH are located initially, at the interface between two nodes in the center of the domain (Figure 4). We set the index *i* for the first node landward of the origin to be equal to zero. The value of *i* increases as we move seaward, and decreases and becomes negative as we move landwards. In general, we can express the location of node *i* as $x_i = (i - 0.5) \cdot \Delta x$.

We discretize equation (11) at node i using the following finite differences form

$$H_{i,j+1} = H_{i,j} + \frac{\Delta t}{\Delta x} \cdot \left(q_{i+\frac{1}{2},j} - q_{i-\frac{1}{2},j} \right) \tag{13}$$

where the superscript *j* refers to the time step, and the subscript *i+1/2* refers to the interface between nodes *i* and *i+1*. This equation guarantees that sediment is conserved in every node of the entire domain. Additionally, we compute the flux from node i to node *i+1* at time step *j* as

$$q_{i+\frac{1}{2},j} = \min\left(H_{i,j} \frac{\Delta x}{\Delta t} + q_{i-\frac{1}{2},j}, \frac{h_{i,j} - h_{i+1,j}}{\Delta x} \right). \tag{14}$$

We note that the formulation introduced by equation (14) departs from the formulation introduced by Lorenzo-Trueba and Voller (2010) (i.e., $q_{i+\frac{1}{2},j} = \min(R_{ab}, (h_{i,j} - h_{i+1,j})/\Delta x)$). Lorenzo-Trueba and Voller's formulation only works when the ABT solely migrates landwards and sediment deposition takes place along the fluvial surface on every cell and time step. Consequently, in this particular scenario sediment flux q is bounded above by the upstream sediment supply in dimensionless form (i.e., $q \leq R_{ab}$). In the more general case presented here, however, we can simulate sediment erosion on the fluvial surface, as well as seaward migration of the ABT. In this case, under the assumption of a non-erodible basement, sediment flux $q_{i+\frac{1}{2},j}$ is bounded above by the sum of the sediment input to the upstream cell $q_{i-\frac{1}{2},j}$ and the total sediment volume in the upstream cell $H_{i,j}\Delta x/\Delta t$.

In order to guarantee stability, the time and space steps need to satisfy $\Delta t/\Delta x^2 < 0.5$. To meet this stability criterion, we generally use a space step $\Delta x = 0.01$ and a time step in the range $10^{-5} \leq \Delta t \leq 5 \cdot 10^{-5}$. Higher resolution may be needed to ensure accuracy for high values of R_{ab}.

At each time step, the solution of (13) explicitly provides new values for the sediment thickness $H_{i,j+1}$ at each node. We then calculate the values at the new time step for the sediment heights $h_{i,j+1}$ from the discrete form of equation (12). With this information, we can calculate the sediment fluxes using equation (14), and move to the next time step to solve again equation (13).

Additionally, although not required, we can determine the position of the ABT at each time step by searching left to right through the domain and finding the first cell i where $q_{i-\frac{1}{2},j} \neq q_{i+\frac{1}{2},j}$. This cell represents the most landward location where sediment deposition occurs, i.e., the cell immediately seaward of the ABT. We then estimate the ABT position by interpolating between nodes i and $i-1$ as follows:

$$r_j = \frac{h_{i,j}+Z_j+R_{ab}x_i}{1-R_{ab}} \,. \qquad (15)$$

We can also estimate the location of the SH at each time step. Under SH progradation, the current total sediment field $H_{i,j}$ is searched, and the first node i where $0 < H_{i,j} + E_i < Z_j$ is located. The SH position is then determined by interpolation through the control volume around node i, i.e.

$$s_j = (i-1)\Delta x - \frac{H_{i,j}}{E_i - Z_j}\Delta x \; . \tag{16}$$

4. Verification of the enthalpy method

We verify the proposed model under two sea-level change scenarios that admit closed form analytical solutions: square-root sea-level rise and fall, and constant sea-level rise. Under the condition of sea-level change proportional to the square root of time i.e., Z= $2\lambda_z\sqrt{t}$, Lorenzo-Trueba et al. (2013) developed an analytical similarity solution in which the movements of the ABT and SH are given by equations of the form: $r = -2\lambda_{ab}\sqrt{t}$ and $s = 2\lambda_{sh}\sqrt{t}$, where λ_{ab} and λ_{sh} are constants determined through the solution of two algebraic equations (Lorenzo-Trueba et al., 2013). We use this analytical solution to assess accuracy of the enthalpy method under a wide range of λ_z and R_{ab} scenarios (see Appendix). In this section, we present two examples that demonstrate model performance under both ABT seaward and landward migration, including their profile evolution (Figure 5).

Under a constant sea-level rise rate $\dot{z}$ (i.e., sea level is described as $Z = \dot{z} \cdot t$), the system eventually reaches a point at which all incoming sediment deposit on the fluvial surface in order to keep pace with sea-level rise (Muto, 2001; Parker and Muto, 2003) , which results in the fluvial plain abandoning the foreset or submarine portion (Figure 2b). When this happens, the system first enters a transition period in which the length of the fluvial plain increases and both the ABT and the SH migrate landwards. This transition period ends when the fluvial surface attains a fixed geometry, and both the ABT and the SH attain a constant landward migration rate. At this point, the geometry of the fluvial surface, as well as the ABT and SH trajectories, can be described analytically (a full derivation of this solution is included in the Appendix). We use this analytical solution to test the fixed grid numerical scheme for a wide range of R_{ab} and $\dot{z}$ values. In all scenarios, there is agreement between the analytical and numerical solutions (see Appendix).

5. System response to sea-level cycles: The importance of fluvial surface dynamics

Numerous studies over the past few decades present sea-level change as the most important allogenic (i.e., external) forcing affecting coastal areas such as fluvial deltas and coastal margins (Blum et al., 2013; Catuneanu et al., 2009; Van Wagoner et al., 1990; Van Wagoner and Bertram, 1995), and consequently as the primary control on stratigraphic architecture. While evidence for incised (paleo) valley systems formed during oscillations in sea level during the Quaternary is extensive (Blum et al., 2013; Blum and Törnqvist, 2000), the range of sea-level cycle amplitudes and frequencies stored in the stratigraphic record remains unclear (Li et al., 2016). In this section, we demonstrate how the proposed enthalpy method can be used to bring some light to this question by exploring the dynamics and stratigraphy of the system under sea-level variations. In particular, we go beyond the scenarios investigated in the model verification and explore the system response under sinusoidal sea-level cycles, i.e.,

$$Z = A\sin(B \cdot t) \quad (17)$$

where *A* and *B* are the dimensionless amplitude and frequency (i.e., 1/period) of the sea-level cycles. We select a representative length scale $l = 100$km, a basement slope $\beta = 10^{-3}$, and a diffusivity ν = $10^5 m^2 y^{-1}$ associated with a catchment length of ~100 km (Swenson et al., 2000). In this way, we can use the dimensional scaling described in equation (4) to calculate the amplitude and period of sea-level cycles using the *A* and *B* values. For instance, *A*=1 and *B*=1 correspond to sea-level cycles of 100m in amplitude and a period of 100,000 years, which are comparable to quaternary-scale eccentricity-driven eustatic sea level cycles (Hajek and Straub, 2017). Lower *A* and *B* values (e.g., *A=0.3* and *B=0.4*) better match with late Miocene conditions, when obliquity cycles (~ 40 ky) resulted in sea changes with ranges of 10–35 m.

An interesting feature under sea-level cycles is that the SH can reverse its direction of migration. During these reversals, the geometric configuration of the system shifts between the one shown in Figure 2a, in which wedge geometry is maintained, and Figure 2b, in which the foreset and the fluvial plain abandons the submarine portion (i.e., autobreak). This is well illustrated in Figures 6 and 7, which demonstrate that the geomorphic enthalpy method introduced here can account for transgression followed by regression and vice versa. Figure 6 includes three stratigraphic profiles produced by the model that demonstrate the effect of R_{ab} on the system response. As we increase R_{ab}, which is proportional to the sediment supply (see equation (5)), the magnitude and occurrence of river incision (i.e., ABT seaward migration) and SH transgression are reduced, and there is larger preservation of sedimentary deposits. The formation and evolution of each of these stratigraphic profiles is included in the supplementary material, and Figure 7a includes the ABT and SH trajectories for the scenario depicted in Figure 6c (medium R_{ab} value).

Figures 6 and 7 (and videos in the supplementary material) also illustrate the importance of the dynamics of the fluvial surface on the ABT and SH responses. During the sea-level rise phase, the relief of the fluvial surface decreases and its convexity increases as a large fraction of the sediment input deposits on the subaerial portion of the sedimentary prism. In contrast, under sea-level fall the relief and concavity of the fluvial surface increase as a larger fraction of sediments bypass the subaerial portion of the delta to build the foreset. These shifts in the curvature and relief of the fluvial surface can delay the response of the system to sea-level variations. In particular, the transition from a concave and seaward migrating fluvial surface profile during sea-level fall to a convex and lower relief fluvial surface during the sea-level rise can result in river incision during the sea-level rise (Figures 6-7a); Lorenzo-Trueba et al. (2013) first reported this interesting phenomenon. Additionally, the transition from a convex fluvial surface profile during the sea-level rise stage to a concave profile during the sea-level fall stage can result in the truncation of sediment layers in the nearshore region, leaving 'lenses' of older sediment surrounded by newer sediments (Figure 6). It is important to note that neither of these two behaviors can be captured by models that impose a linear fluvial slope (Kim and Muto, 2007; Lorenzo-Trueba et al., 2012), or the general sequence stratigraphic model, which assumes a fixed fluvial surface profile that translates seaward and landward, tracking the regressing and transgressing SH (Posamentier and Vail, 1988).

To further explore the time lags in system response, we define the ABT and SH residuals (i.e., s_{res} and r_{res}) as the difference between the ABT and SH trajectories under sea-level cycles and the corresponding trajectories under constant sea level (Figure 7a). By plotting the residual trajectories with the sea-level curve (Figure 7b and 7c), we find that SH response is typically in phase with sea level such that maxima and minima in the SH trajectory correspond approximately to minima and maxima in sea level, respectively. In contrast, delays in the ABT response to sea-level variations can be geologically long-lived, and can result in river incision that prolongs into the sea-level rise stage (Figure 8 and 9). Such time delays increase as R_{ab} increases, and can reach values of hundreds of thousands of years, but barely change as a function of the amplitude of the sea-level oscillations *A* (Figure 8a). River incision during sea-level rise, however, can only occur when *A* is at least large enough to cause river incision during the fall stage, which can then extend into the sea-level rise stage. Thus, the total sediment volume eroded (i.e., river incision) under sea-level rise increases as *A* increases (Figure 8b), and represents a significant fraction of the total sedimentary wedge volume under high amplitude sea-level oscillations (Figure 9).

The relationship between the sediment volume eroded during sea-level rise and R_{ab} is more complex (Figure 8b). Under low to medium values of R_{ab}, the seaward migration of the ABT drives river incision (Figure 9b and 9c). In this case, as R_{ab} increases, the longer the seaward migration of the ABT prolongs beyond the sea-level fall stage into the sea-level rise stage, which in turn results in a higher sediment volume eroded. Under medium to high values of R_{ab}, however, the ABT can maintain its landward migration even under extended periods of sea-level fall, and river incision occurs instead due to curvature changes of the fluvial surface (Figure 9d). In this scenario, an increase in R_{ab}, which is proportional to the sediment supply (see equation (5)), tends to reduce the sediment volume eroded under sea-level cycles.

6. Discussion and future work

Numerous field, experimental, and theoretical studies have been conducted to date to understand how allogenic controls such as sea-level change influence stratigraphy (Allen, 1978; Armitage et al., 2011; Heller et al., 2001; Heller and Paola, 1996; Hickson et al., 2005; Martin et al., 2011, 2009; van Heijst and Postmal, 2001; Van Wagoner et al., 1990). Despite all these efforts, which provide a sound conceptual framework for interpreting ancient deposits, there exist fundamental gaps regarding the relationship between processes, stratigraphy, and fluvial-deltaic evolution. In this manuscript, we address this knowledge gap by developing and verifying a fixed grid enthalpy-like numerical solution aimed to explore the evolution of fluvial deltas under a wide range of scenarios. The novelty of this modeling framework, which can be viewed as a generalized one-dimensional Stefan problem with two geomorphic moving boundaries (i.e., the ABT and the SH), is that the "latent heat" (which resembles ocean depth in our case) can change both in time and space. As a result, this model can for the first time incorporate sea-level cycles, as well as cycles of SH transgression/regression.

Model results in this manuscript do not aim at specifically reproducing the evolution of any particular fluvial delta, and therefore do not capture the complexities associated with multiple grain sizes, sediment compaction, or deep crustal processes. The model also assumes that the evolution of the system can be described in a one-dimensional longitudinal section, leaving out processes such as river avulsions, which can play a role on the large-scale evolution of the system. These model simplifications, however, allow us to focus our analysis on the interplay between sediment supply, sea-level changes, and the dynamics of the fluvial surface. Additionally, given the simplicity of the model we can explore the effect of this interplay under a wide range of system parameters.

Overall, model results demonstrate the potential of numerical heat transfer methods, specifically those developed to solve moving boundary problems, to advance our understanding of the formation and evolution of sedimentary basins. Model results also demonstrate that the dynamics of the fluvial surface can play an essential role on the system response to sea-level variations. Previous studies have highlighted the importance of autogenic storage and release processes during a full sea-level cycle, such that periods of sea-level rise are not purely depositional while periods of sea-level fall are also not purely erosional (Blum and Price, 1998; Holbrook, 2001; Strong and Paola, 2008). To the best of our knowledge, however, this is the first study that relates changes in the relief and concavity of the fluvial surface profile during sea-level cycles with the occurrence of geologically long-lived (i.e., thousands of years) river incision during sea-level rise. Moreover, the model predicts that the volume of sediment eroded during river incision under sea-level rise significantly increases as the amplitude of the sea-level oscillations increase. Future work will aim at narrowing down the conditions and past sea-level changes that could make such behavior likely. Additionally, we are planning to carry out laboratory-scale flume experiments to validate the model results. The next step in terms of numerical modeling will be to extend the geomorphic enthalpy model into two dimensions.

Acknowledgments

We thank the donors of the American Chemical Society Petroleum Research Fund for support of this research (PRF #58817-DNI8). We also thank two anonymous reviewers for their valuable comments.

Computer Code Availability

The code “1D enthalpy method”, developed by William Anderson and Jorge Lorenzo-Trueba can be accessed since October 2018 at https://github.com/JorgeMSU/1D-enthalpy-method. For details about this code, contact Jorge Lorenzo-Trueba via email (lorenzotruej@montclair.edu) or by phone (973-655-5320). Jorge Lorenzo-Trueba’s office is at 1 Normal ave., Motntclair State University, NJ 07043. The code is less than 200 lines, it can run in a standard laptop, and is written in matlab.

Appendix A: Additional verification of the enthalpy method.

In this section, we include further testing of the fixed grid numerical scheme under two sea-level change scenarios that admit closed form analytical solutions: square-root sea-level rise and fall, and constant sea-level rise.

A.1 Square-root sea-level rise and fall

Under the condition of sea-level change proportional to the square root of time i.e., Z= $2\lambda_z\sqrt{t}$, Lorenzo-Trueba et al. (2013) developed an analytical similarity solution in which the movements of the ABT and SH are given by equations of the form:

$$r = -2\lambda_{ab}\sqrt{t} \quad \text{(A1a)}$$

$$s = 2\lambda_{sh}\sqrt{t} \quad \text{(A1b)}$$

where λ_{ab} and λ_{sh} are constants determined through the solution of two algebraic equations (Lorenzo-Trueba et al., 2013). We use this analytical solution to assess accuracy of the enthalpy method under a wide range of R_{ab} and λ_Z values. Figure 5 shows plots of the SH and ABT trajectories over time for two values of R_{ab} during sea-level fall. In both scenarios, there is agreement between the analytical and numerical solutions. Depending on both R_{ab} and the value of λ_Z the delta can undergo coastal offlap or coastal onlap during sea-level fall. The profile evolutions in figure 5 illustrate differences in concavity of the fluvial surface that are a result of the direction of ABT migration. In scenarios of sea-level fall proportional to the square root of time larger values of R_{ab} or smaller values of λ_Z result in coastal onlap and a concave up fluvial surface. However, significantly decreasing R_{ab} or increasing the magnitude of λ_Z causes the delta to undergo coastal offlap and produces a concave down fluvial surface. During costal offlap sediments are reworked in the upstream portion of the delta and provided to the rest of the system causing sediment flux values in the fluvial surface to exceed R_{ab} and resulting in the concave downward profile. Model runs for several values of R_{ab} and λ_Z are included in figures A1 and A2.

A further test of the robustness of the enthalpy solution is revealed by investigating its performance across the entire feasible range of the ABT slope ratio $0 < R_{ab} < 1$; in each case the value of λ_Z is set proportional to λ_{sh}. First, the analytical solution in Lorenzo-Trueba et al. 2012 is used to predict values of λ_{ab} and λ_{sh}. Then, we extract the values of λ_{ab} and λ_{sh} at specific values of $R_{ab}[0.05{:}\,0.05{:}\,0.95]$ through fitting the forms in (9) to the predicted trajectories r and s given by the enthalpy solution. Benchmarks are made for both a sea-level rise (e.g., $\lambda_Z = 0.5\lambda_{sh}$) and a sea-level fall (e.g., $\lambda_Z = -0.5\lambda_{sh}$). In Figure A3 we present a comparison of the analytical values of the moving boundary parameters (solid-line) with those predicted by the enthalpy method (shapes). We find that across a wide range of conditions the time stepping solution matches the analytical solution.

A.2 <u>Constant sea-level rise</u>

Under a constant sea-level rise rate $\dot{z}$ (i.e., sea level is described as $Z = \dot{z} \cdot t$), the system can reach a point in which the incoming sediment flux is insufficient to supply the foreset (Muto, 2001; Parker and Muto, 2003), which results in the fluvial plain abandoning the submarine portion (Figure 2b). When this happens, the system first enters a transition period in which the length of the fluvial plain increases and both the ABT and the SH migrate landwards. This transition period ends when the fluvial surface attains a fixed geometry, and both the ABT and the SH attain a constant landward migration rate. At this point, the problem admits an analytical solution as the fluvial-surface attains a fixed geometry that migrates landwards at a given speed. We can then describe such analytical solution by setting the following similarity variable:

$$\xi = x + \dot{z}t, \tag{A2a}$$

scale the sediment height by

$$\eta = h - \dot{z}t, \tag{A2b}$$

and define the following location for the boundaries of the fluvial surface

$$s^* = s_i - \dot{z}t \tag{A3a}$$

$$r^* = r_i - \dot{z}t \; . \tag{A3b}$$

In this way, the similarity solution becomes

$$\frac{d^2\eta}{d\xi^2} - \dot{z}\frac{d\eta}{d\xi} - \dot{z} = 0\,, \qquad r^* \le \xi \le s^* \tag{A4}$$

with boundary conditions

$$\eta|_{\xi=s^*} = 0 \tag{A5a}$$

$$\eta|_{\xi=r^*} = -r^* \tag{A5b}$$

$$\left.\frac{\partial\eta}{\partial\xi}\right|_{\xi=r^*} = -R_{ab} \tag{A5c}$$

$$\left.\frac{\partial\eta}{\partial\xi}\right|_{\xi=s^*} = 0\,. \tag{A5d}$$

On satisfying (A3), (A4a), and (A4d) we obtain the following solution

$$\eta = \frac{1}{\dot{z}}\exp(\dot{z}\xi - \dot{z}s^*) - \xi + \frac{R_{ab}-1}{\dot{z}} \tag{A6a}$$

$$h = \frac{1}{\dot{z}}\exp(\dot{z}x - \dot{z}s) - x + \frac{R_{ab}-1}{\dot{z}}\,. \tag{A6b}$$

From (2) and (3) we obtain the values of s*, and r*

$$s^* = \frac{R_{ab}}{\dot{z}} \tag{A7a}$$

$$r^* = \frac{1}{\dot{z}}[R_{ab} + \ln(1 - R_{ab})]\,. \tag{A7b}$$

Thus, the length of the fluvial surface can be calculated as

$$s^* - r^* = s_i - r_i = \frac{\ln(1-R_{ab})}{\dot{z}}. \tag{A8}$$

We use this analytical solution to test the fixed grid numerical scheme for a wide range of R_{ab} and $\dot{Z}$ values. Figure A4 shows plots of the movement of the SH and ABT over time. We find that the trajectories predicted by the enthalpy solution (solid-lines) eventually match the analytical solution (dashed-line).

Additionally, further test of the robustness of the enthalpy solution is revealed by investigating its performance across the entire feasible range of the ABT slope ratio $0 < R_{ab} < 1$. In particular, we calculate the length of the fluvial surface at steady state (i.e., *s*-*r*) for specific values of $R_{ab}[0.05\colon 0.05\colon 0.95]$, using the enthalpy solution and the analytical solution (equation (A7)). In Figure A5 we present a comparison of the analytical values of the moving boundary parameters (solid-line) with those predicted by the enthalpy method (shapes). We find that across a wide range of conditions the time stepping solution matches the analytical solution.

References

Allen, J.R.L., 1978. Studies in fluviatile sedimentation: an exploratory quantitative model for the architecture of avulsion-controlled alluvial suites. Sediment. Geol. 21, 129–147. https://doi.org/10.1016/0037-0738(78)90002-7

An, C., Cui, Y., Fu, X., Parker, G., 2017. Gravel-bed river evolution in earthquake-prone regions subject to cycled hydrographs and repeated sediment pulses. Earth Surf. Process. Landforms 42, 2426–2438. https://doi.org/10.1002/esp.4195

Armitage, J.J., Duller, R.A., Whittaker, A.C., Allen, P.A., 2011. Transformation of tectonic and climatic signals from source to sedimentary archive. Nat. Geosci. 4, 231–235. https://doi.org/10.1038/ngeo1087

Blum, M., Martin, J., Milliken, K., Garvin, M., 2013. Paleovalley systems: Insights from Quaternary analogs and experiments. Earth-Science Rev. 116, 128–169. https://doi.org/10.1016/j.earscirev.2012.09.003

Blum, M.D., Price, D.M., 1998. Relative Role of Eustasy, Climate, and Tectonism in Continental Rocks. Quat. Alluv. Plain Constr. Response to Glacio-eustatic Clim. Control. Texas Gulf Coast. Plain 59, 31–48.

Blum, M.D., Törnqvist, T.E., 2000. Fluvial responses to climate and sea-level change: A review and look forward. Sedimentology 47, 2–48. https://doi.org/10.1046/j.1365-3091.2000.00008.x

Capart, H., Bellal, M., Young, D.-L., 2007. Self-Similar Evolution of Semi-Infinite Alluvial Channels with Moving Boundaries. J. Sediment. Res. 77, 13–22. https://doi.org/10.2110/jsr.2007.009

Capart, H., Hsu, J., Lai, S., Hsieh, M., 2010. Formation and decay of a tributary-dammed lake, Laonong River, Taiwan. Water Resour. Res. 46.

Catuneanu, O., Abreu, V., Bhattacharya, J.P., Blum, M.D., Dalrymple, R.W., Eriksson, P.G., Fielding, C.R., Fisher, W.L., Galloway, W.E., Gibling, M.R., Giles, K.A., Holbrook, J.M., Jordan, R., Kendall, C.G.S.C., Macurda, B., Martinsen, O.J., Miall, A.D., Neal, J.E., Nummedal, D., Pomar, L., Posamentier, H.W., Pratt, B.R., Sarg, J.F., Shanley, K.W., Steel, R.J., Strasser, A., Tucker, M.E., Winker, C., 2009. Towards the standardization of sequence stratigraphy. Earth-Science Rev. 92, 1–33. https://doi.org/10.1016/j.earscirev.2008.10.003

Chavarrías, V., Blom, A., Orrú, C., Martín-Vide, J.P., Viparelli, E., 2018. A Sand-Gravel Gilbert Delta Subject to Base Level Change. J. Geophys. Res. Earth Surf. 123, 1160–1179. https://doi.org/10.1029/2017JF004428

Crank, J., 1984. Free and Moving Boundary Problems. Oxford Press.

Edmonds, D.A., Paola, C., Hoyal, D.C.J.D., Sheets, B.A., 2011. Quantitative metrics that describe river deltas and their channel networks. J. Geophys. Res. Earth Surf. 116, 1–15. https://doi.org/10.1029/2010JF001955

Fagherazzi, S., Overeem, I., 2007. Models of Deltaic and Inner Continental Shelf Landform Evolution. Annu. Rev. Earth Planet. Sci. 35, 685–715. https://doi.org/10.1146/annurev.earth.35.031306.140128

Hajek, E.A., Straub, K.M., 2017. Autogenic Sedimentation in Clastic Stratigraphy. Annu. Rev. Earth Planet. Sci. 45, 681–709. https://doi.org/10.1146/annurev-earth-063016-015935

Heller, P.L., Paola, C., 1996. Downstream Changes in Alluvial Architecture: An Exploration of Controls on Channel-Stacking Patterns. J. Sediment. Res. 66, 297–306. https://doi.org/10.1306/D4268333-2B26-11D7-8648000102C1865D

Heller, P.L., Paola, C., Hwang, I.G., John, B., Steel, R., 2001. Geomorphology and sequence stratigraphy due to slow and rapid base-level changes in an experimental subsiding basin (XES96-1). Am. Assoc. Pet. Geol. Bull. 85, 817–838. https://doi.org/10.1306/8626CA0F-173B-11D7-8645000102C1865D

Henriksen, S., Hampson, G.J., Helland-Hansen, W., Johannessen, E.P., Steel, R.J., 2009. Shelf edge and shoreline trajectories, a dynamic approach to stratigraphic analysis. Basin Res. 21, 445–453. https://doi.org/10.1111/j.1365-2117.2009.00432.x

Hickson, T.A., Sheets, B.A., Paola, C., Kelberer, M., 2005. Experimental Test of Tectonic Controls on Three-Dimensional Alluvial Facies Architecture. J. Sediment. Res. 75, 710–722. https://doi.org/10.2110/jsr.2005.057

Holbrook, J., 2001. Origin, genetic interrelationships, and stratigraphy over the continuum of fluvial channel-form bounding surfaces: An illustration from middle Cretaceous strata, Southeastern Colorado. Sediment. Geol. 144, 179–222. https://doi.org/10.1016/S0037-0738(01)00118-X

Kim, W., Muto, T., 2007. Autogenic response of alluvial-bedrock transition to base-level variation: Experiment and theory. J. Geophys. Res. Earth Surf. 112, 1–13. https://doi.org/10.1029/2006JF000561

Lai, S.Y.J., Capart, H., 2007. Two-diffusion description of hyperpycnal deltas. J. Geophys. Res. Earth Surf. 112. https://doi.org/10.1029/2006JF000617

Lai, S.Y.J., Hsiao, Y.T., Wu, F.C., 2017. Asymmetric Effects of Subaerial and Subaqueous Basement Slopes on Self-Similar Morphology of Prograding Deltas. J. Geophys. Res. Earth Surf. 122, 2506–2526. https://doi.org/10.1002/2017JF004244

Li, Q., Yu, L., Straub, K.M., 2016. Storage thresholds for relative sea-level signals in the stratigraphic record. Geology 44, 179–182.

Lorenzo-Trueba, J., Voller, V.R., 2010. Analytical and numerical solution of a generalized Stefan problem exhibiting two moving boundaries with application to ocean delta formation. J. Math. Anal. Appl. 366, 538–549. https://doi.org/10.1016/j.jmaa.2010.01.008

Lorenzo-Trueba, J., Voller, V.R., Muto, T., Kim, W., Paola, C., Swenson, J.B., 2009. A similarity solution for a dual moving boundary problem associated with a coastal-plain depositional system. J. Fluid Mech. 628, 427–443. https://doi.org/10.1017/S0022112009006715

Lorenzo-Trueba, J., Voller, V.R., Paola, C., 2013. A geometric model for the dynamics of a fluvially dominated deltaic system under base-level change. Comput. Geosci. 53, 39–47. https://doi.org/10.1016/j.cageo.2012.02.010

Lorenzo-Trueba, J., Voller, V.R., Paola, C., Twilley, R.R., Bevington, A.E., 2012. Exploring the role of organic matter accumulation on delta evolution. J. Geophys. Res. Surf. 117, F00A02. https://doi.org/10.1029/2012JF002339

Marr, J.G., Swenson, J.B., Paola, C., Voller, V.R., 2000. A two-diffusion model of fluvial stratigraphy in closed depositional basins. Basin Res. 12, 381–398. https://doi.org/10.1111/j.1365-2117.2000.00134.x

Martin, J., Cantelli, A., Paola, C., Blum, M., Wolinsky, M., 2011. Quantitative Modeling of the Evolution and Geometry of Incised Valleys. J. Sediment. Res. 81, 64–79. https://doi.org/10.2110/jsr.2011.5

Martin, J., Paola, C., Abreu, V., Neal, J., Sheets, B., 2009. Sequence stratigraphy of experimental strata under known conditions of differential subsidence and variable base level. Am. Assoc. Pet. Geol. Bull. 93, 503–533. https://doi.org/10.1306/12110808057

Muto, T., 2001. Shoreline autoretreat substantiated in flume experiments. J. Sediment. Res. 71, 246–254. https://doi.org/10.1306/091400710246

Muto, T., Steel, R.J., 2002. Role of autoretreat and A/S changes in the understanding of deltaic shoreline trajectory: A semi-quantitative approach. Basin Res. 14, 303–318. https://doi.org/10.1046/j.1365-2117.2002.00179.x

Paola, C., 2000. Quantitative models of sedimentary basin filling. Sedimentology. https://doi.org/10.1046/j.1365-3091.2000.00006.x

Paola, C., Heller, P.L., Angevine, C.L., 1992. The large-scale dynamics of grain-size variation in alluvial basins, 1: Theory. Basin Res. 4, 73–90. https://doi.org/10.1111/j.1365-2117.1992.tb00145.x

Paola, C., Voller, V.R., 2005. A generalized Exner equation for sediment mass balance. J. Geophys. Res. Earth Surf. 110, 1–8. https://doi.org/10.1029/2004JF000274

Parker, G., Muto, T., 2003. 1D numerical model of delta reponse to rising sea level. 3rd IAHR Symp. River, Coast. Estuar. Morphodynamics 1–10.

Parker, G., Muto, T., Akamatsu, Y., Dietrich, W.E., Lauer, J.W., 2008. Unravelling the conundrum of river response to rising sea-level from laboratory to field. Part I: Laboratory experiments. Sedimentology 55, 1643–1655. https://doi.org/10.1111/j.1365-3091.2008.00961.x

Posamentier, H.W., Allen, H.W., James, D.P., Tesson, M., 1992. Forced regression in a sequence stratigraphic framework: Concepts, examples, and sequence stratigraphic significance. Am. Assoc. Pet. Geol. Bull. 76, 1687–1709.

Posamentier, H.W., Vail, P.R., 1988. Eustatic Controls on Clastic Deposition IH—Sequence and Systems Tract Models. Sea-Level Chang. 42, 125–154. https://doi.org/10.2110/pec.88.01.0125

Postma, G., Kleinhans, M.G., Meijer, P.T.H., Eggenhuisen, J.T., 2008. Sediment transport in analogue flume models compared with real-world sedimentary systems: A new look at scaling evolution of sedimentary systems in a flume. Sedimentology 55, 1541–1557. https://doi.org/10.1111/j.1365-3091.2008.00956.x

Strong, N., Paola, C., 2008. Valleys That Never Were: Time Surfaces Versus Stratigraphic Surfaces. J. Sediment. Res. 78, 579–593.

Swenson, J.B., Muto, T., 2007. Response of coastal plain rivers to falling relative sea-level: Allogenic controls on the aggradational phase. Sedimentology 54, 207–221. https://doi.org/10.1111/j.1365-3091.2006.00830.x

Swenson, J.B., Paola, C., Pratson, L., Voller, V.R., Murray, A.B., 2005. Fluvial and marine controls on combined subaerial and subaqueous delta progradation: Morphodynamic modeling of compound-clinoform development. J. Geophys. Res. Earth Surf. 110, 1–16. https://doi.org/10.1029/2004JF000265

Swenson, J.B., Voller, V.R., Paola, C., Parker, G., Marr, J.G., 2000. Fluvio-deltaic sedimentation: A generalized Stefan problem. Eur. J. Appl. Math. 11, 433–452.

https://doi.org/10.1017/S0956792500004198

Törnqvist, T.E., Wortman, S.R., Mateo, Z.R.P., Milne, G.A., Swenson, J.B., 2006. Did the last sea level lowstand always lead to cross-shelf valley formation and source-to-sink sediment flux? J. Geophys. Res. Earth Surf. 111. https://doi.org/10.1029/2005JF000425

van Heijst, M.W.I.M., Postmal, G., 2001. Fluvial response to sea-level changes: A quantitative analogue, experimental approach. Basin Res. 13, 269–292. https://doi.org/10.1046/j.1365-2117.2001.00149.x

Van Wagoner, J.C., Bertram, G.T., 1995. Sequence Stratigraphy of Foreland Basin Deposits. Memoir 64, 487.

Van Wagoner, J.C., Mitchum, R.M.J., Campion, K.M., Rahmanian, V.D., 1990. Siliciclastic Sequence Stratigraphy in Well Logs, Cores and Outcrops. AAPG Methods Explor. Ser. 7, 1–55.

Voller, V.R., Swenson, J.B., Kim, W., Paola, C., 2006. An enthalpy method for moving boundary problems on the earth's surface. Int. J. Numer. Methods Heat Fluid Flow 16, 641–654. https://doi.org/10.1108/09615530610669157

Voller, V.R., Swenson, J.B., Paola, C., 2004. An analytical solution for a Stefan problem with variable latent heat. Int. J. Heat Mass Transf. 47, 5387–5390. https://doi.org/10.1016/j.ijheatmasstransfer.2004.07.007

Tables

Table 1. State Variables and their Dimensions

Symbol	**Units**	**Description**	**Dimensionless symbol**
t	T	Time	t
x	L	Horizontal distance	x
h	L	Height above current sea-level	h
r	L	Alluvial-bedrock transition horizontal distance from origin	r
s	L	Shoreline horizontal distance from origin	s
q	$L^2 \cdot T^{-1}$	Sediment flux	q
Z	L	Sea-level	Z
H	-	Enthalpy	H
E	L	Basement elevation	E

Table 2. Description of the input parameters and their dimensionless groups

<table>
<tr><th>Symbol</th><th>Units</th><th>Description</th><th>Dimensionless symbol</th></tr>
<tr><td>q_0</td><td>$L^2 \cdot T^{-1}$</td><td>Sediment flux at ABT</td><td rowspan="3">R_{ab}</td></tr>
<tr><td>ν</td><td>$L^2 \cdot T^{-1}$</td><td>Fluvial diffusivity</td></tr>
<tr><td>β</td><td>-</td><td>Basement slope</td></tr>
</table>

Ψ	-	Foreset slope	R_{sh}
$\dot{z}$	$L \cdot T^{-1}$	Rate of sea-level rise	$\dot{z}$
A	L	Amplitude of sea-level oscillations	A
B	T^{-1}	Frequency of sea-level oscillations	B

Figures

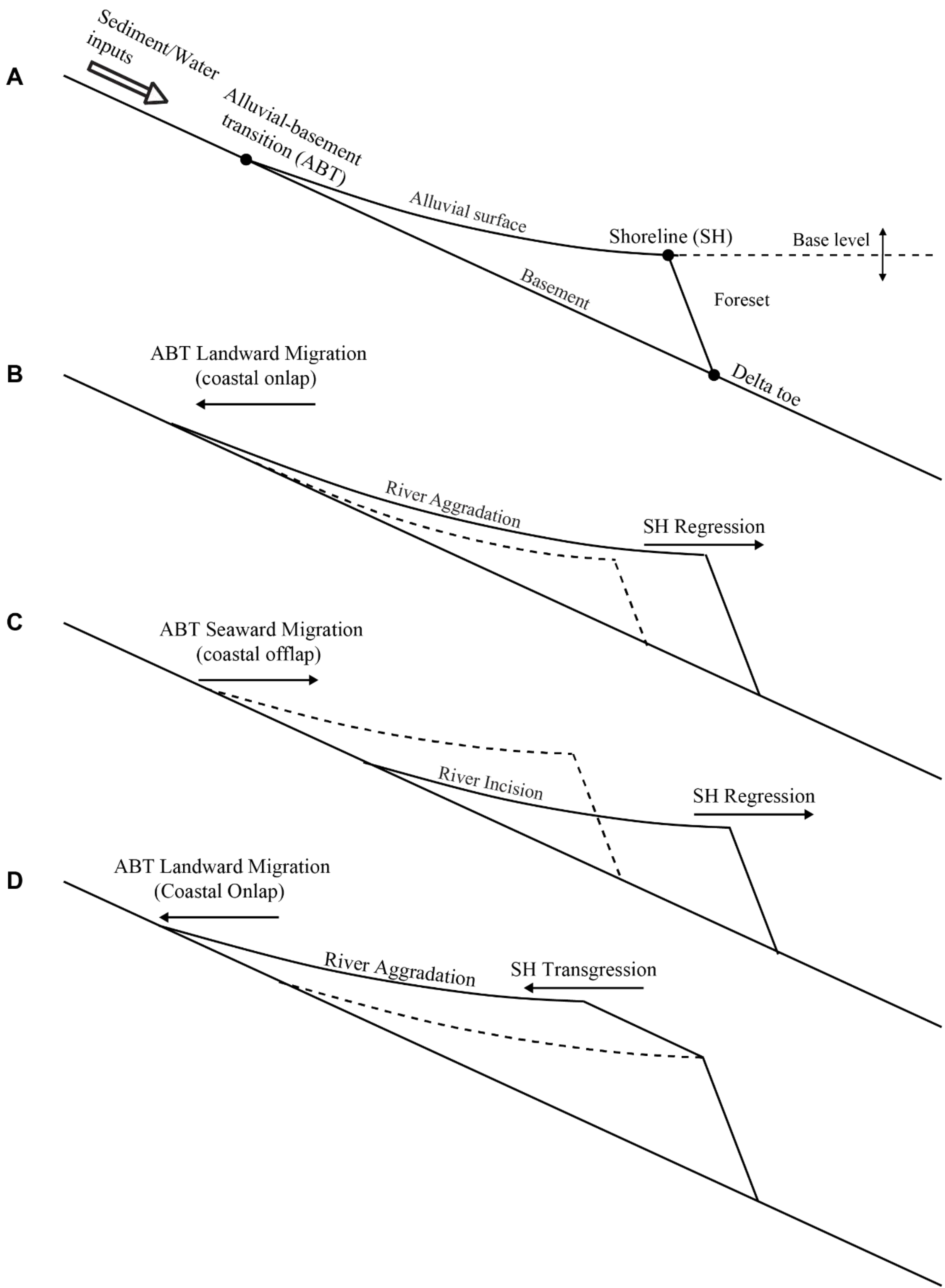

Figure 1. Conceptual sketches of the fluvio-deltaic system illustrating (a) geomorphic moving boundaries and key components, and (b)-(d) shoreline regression/transgression, coastal onlap/offlap at the ABT, and river aggradation/incision. Note the strong exaggeration of the vertical scale.

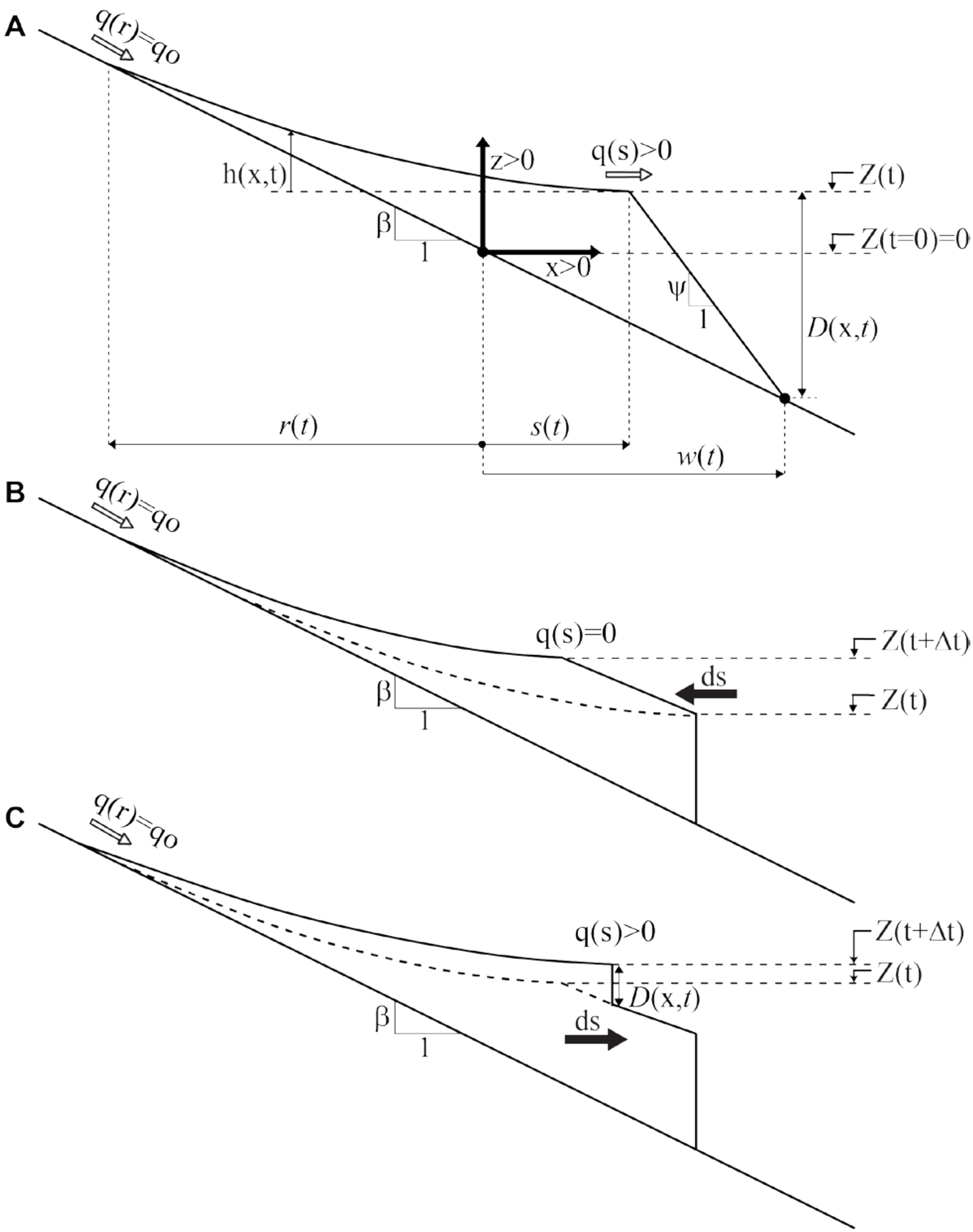

Figure 2. (a) Model setup, including state variables. (b) Sketch for autobreak. (c) Sketch for shoreline regression after autobreak

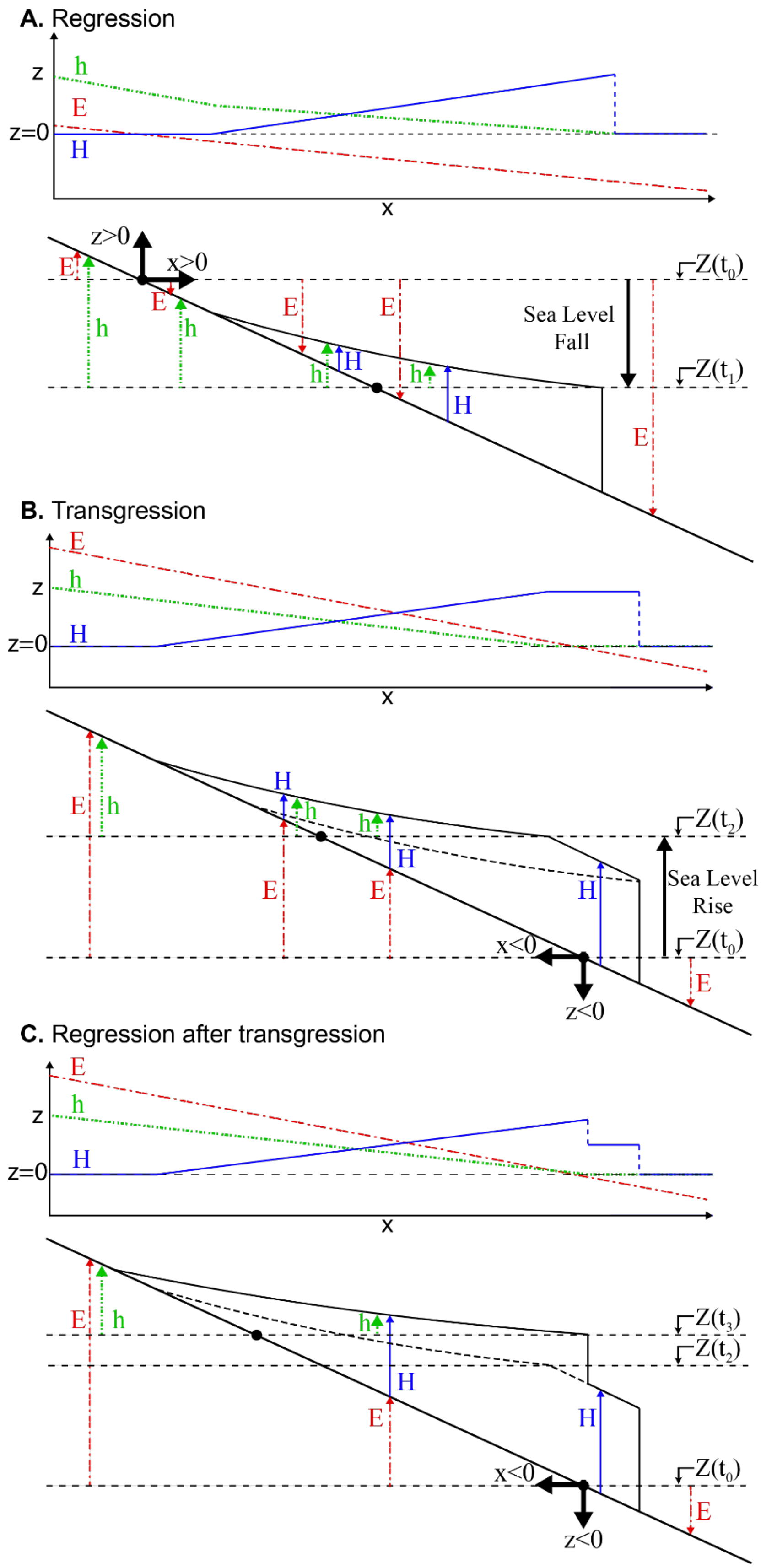

A. Regression
z
h
E
z=0
H
x
z>0
x>0
E
h
Sea Level
Fall
Z(t0)
Z(t1)
B. Transgression
Sea Level
Rise
Z(t2)
x<0
z<0
C. Regression after transgression
Z(t3)

Figure 3. Model variables, including the enthalpy function *H*, the basement elevation *E*, and the fluvial surface elevation respect to the current sea level *h*, under (a) sea-level fall and SH regression, (b) sea-level rise and SH transgression, and (c) SH regression after autobreak.

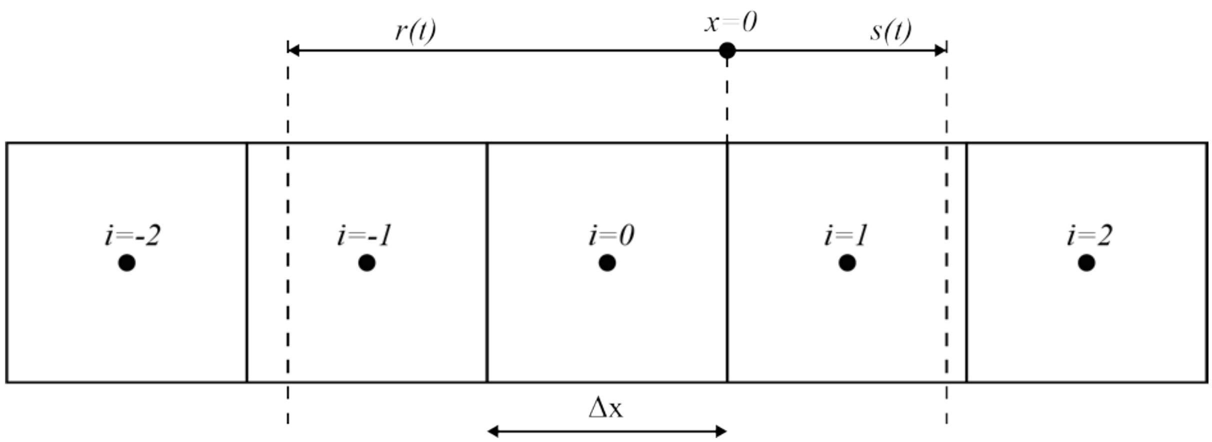

Figure 4. Sketch of discrete domain. In general the locations of the SH and the ABT, *s* and *r* respectively, are in between two nodes of our discrete domain.

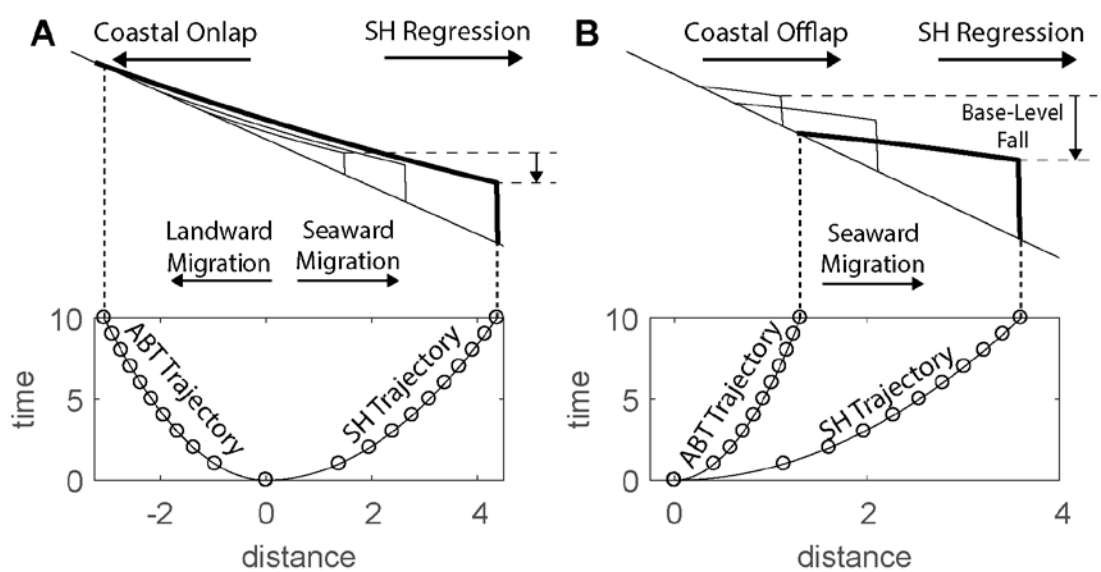

Figure 5. Model runs under square root sea-level fall with (a) $R_{ab} = 0.8$, $\lambda_Z = -0.3$, and (b) $R_{ab} = 0.2$, $\lambda_Z = -0.3$. At the bottom, we include a comparison of boundary trajectories of the analytical (solid-lines) and numerical (circles) solutions. At the top, we depict the evolution of the longitudinal profile over time.

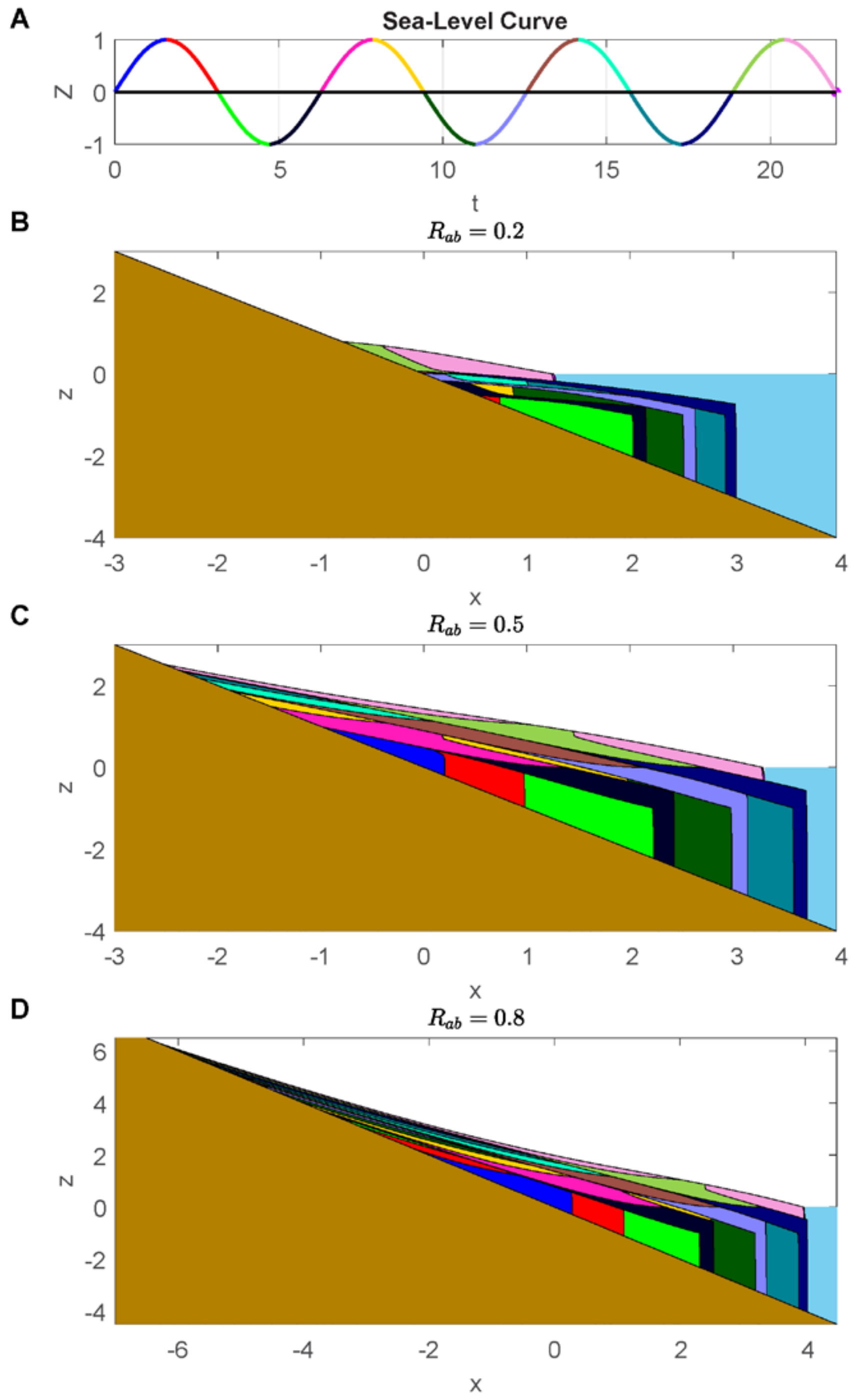

Figure 6. Stratigraphies produced under sea-level cycling for three different values of the dimensionless group $R_{ab} = q_0/(\beta v)$. Videos showing the evolution over time are available in the supplementary material.

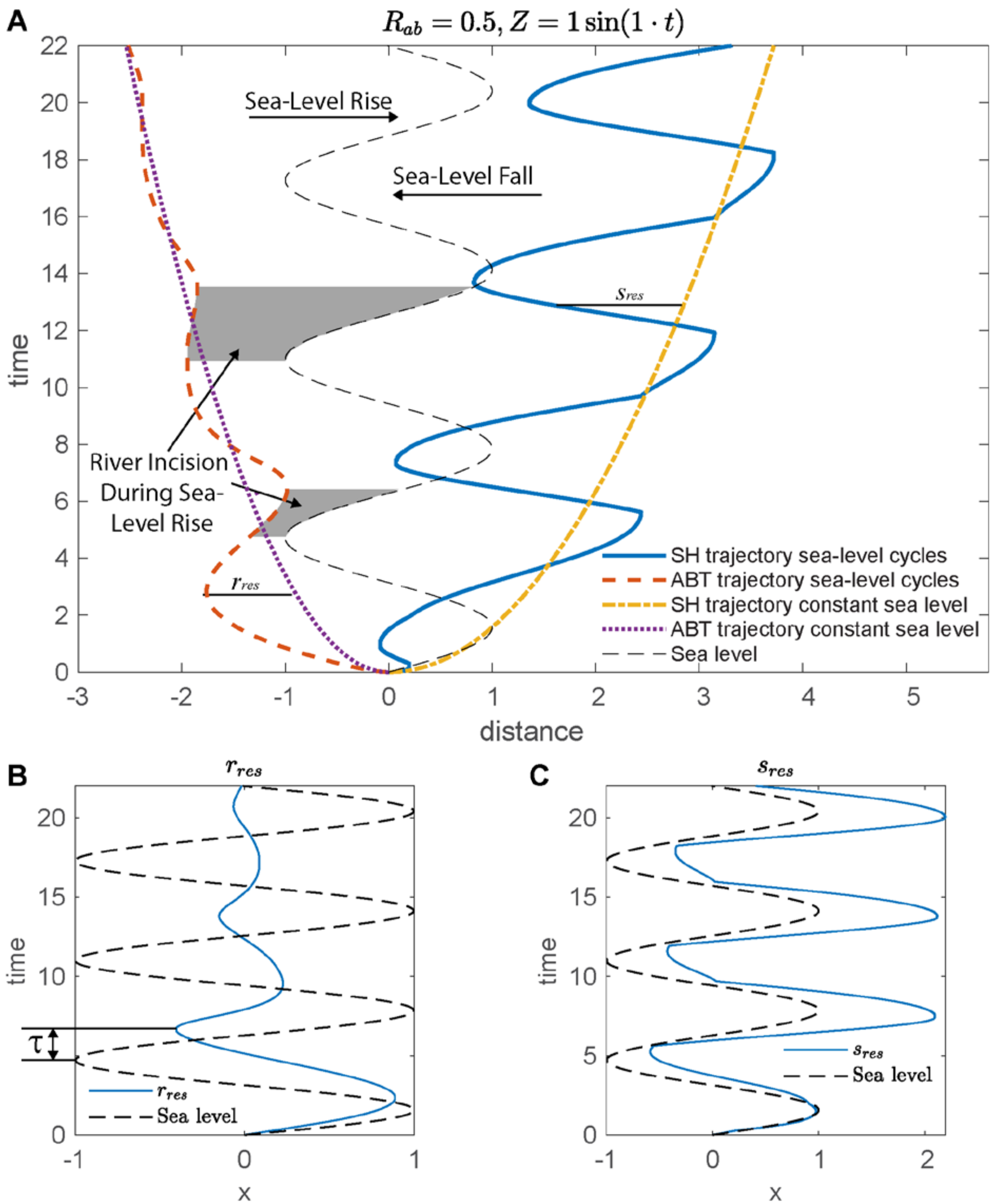

Figure 7. (a) ABT and SH trajectories under sea-level cycles (i.e., $Z = \sin(t)$) and $R_{ab} = 0.5$. Shaded intervals correspond to intervals of river incision during sea-level rise. (b) Plot of ABT residuals, r_{res} , and defining the time lag τ, as a function of the ABT residual. (c) Plot of SH residuals, s_{res}.

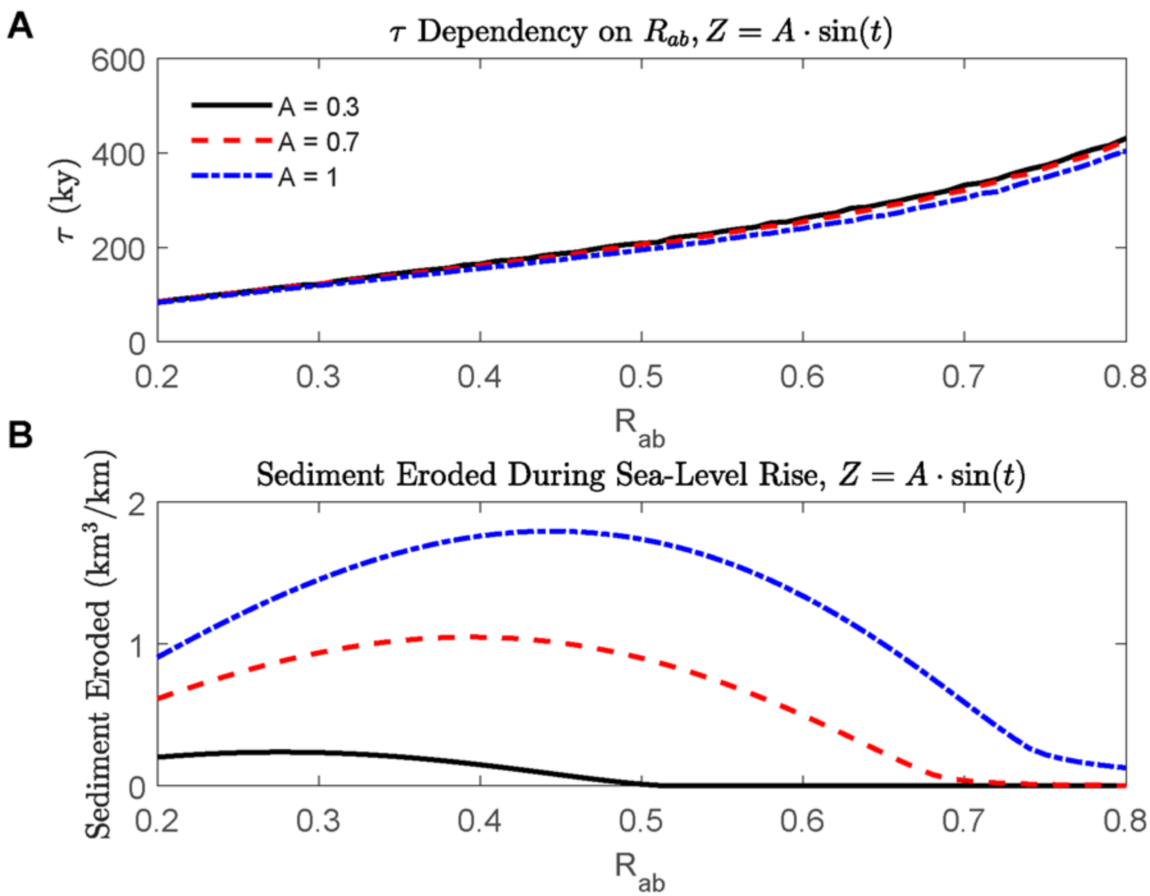

Figure 8. (a) Values for the delay in ABT response to sea-level rise as a function of the dimensionless group $R_{ab} = q_0/(\beta v)$, and the amplitude of the sea-level cycles A. (b) Sediment volume eroded during sea-level rise, also as a function of R_{ab} and A.

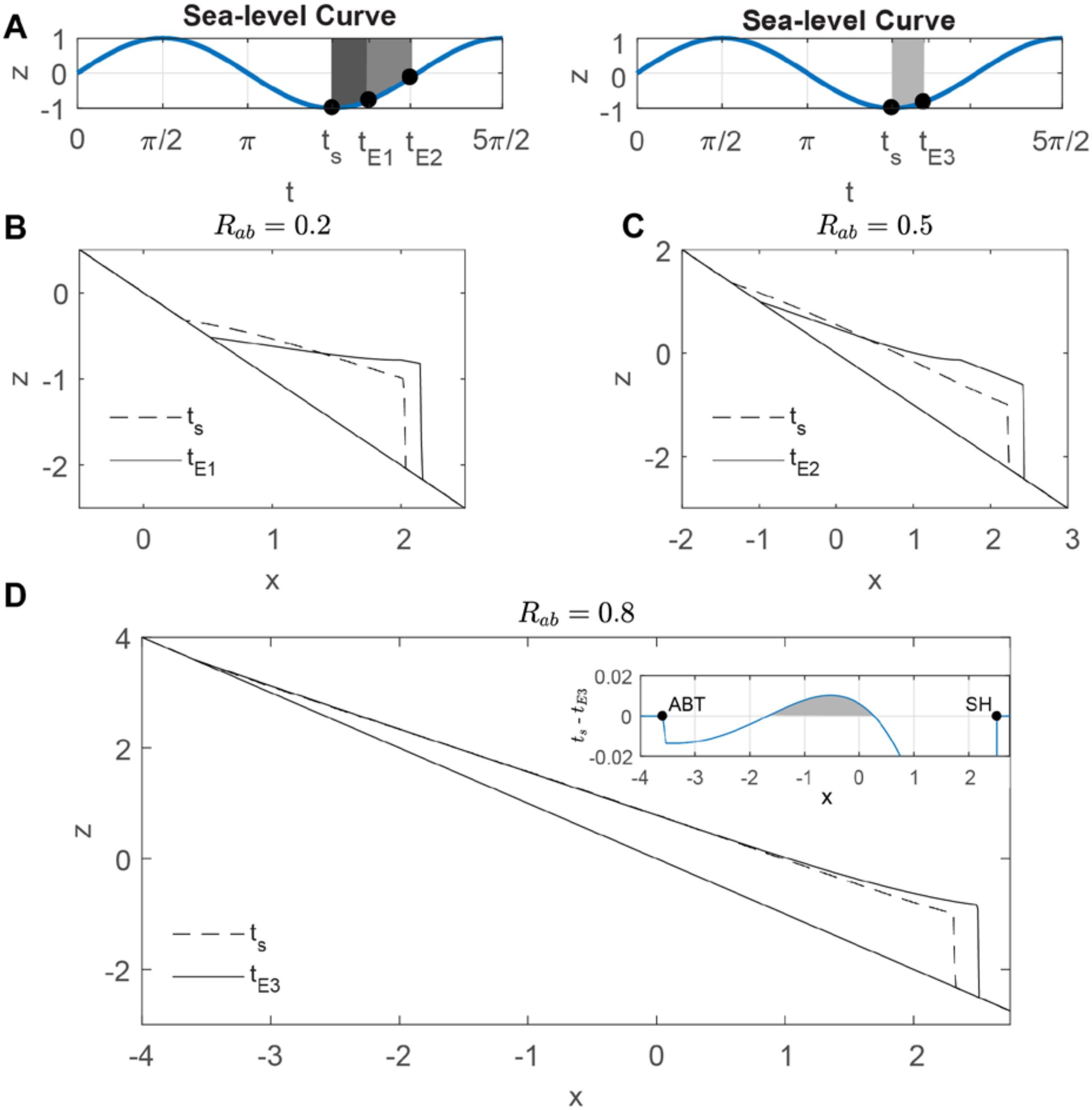

Figure 9. a) Sea-level curves showing the times for the onset of sea-level rise t_s, and at the conclusion of river incision under sea-level rise for different R_{ab} values (i.e., t_{E1} for $R_{ab} = 0.2$, t_{E2} for $R_{ab} = 0.5$, and t_{E3} for $R_{ab} = 0.8$). Below, longitudinal profiles depicting the sections at the onset of sea-level rise (dashed line), and at the conclusion of river incision under sea-level rise (solid line) under (b) $R_{ab} = 0.2$, (c) $R_{ab} = 0.5$, and (d) $R_{ab} = 0.8$. Note that under $R_{ab} = 0.8$, although the ABT does not migrate seawards, sediment erodes from the mid portion of the fluvial surface during sea-level rise. The stratigraphic profiles for the three model runs are included in Figure 6, and the ABT and SH trajectories for the $R_{ab} = 0.5$ scenario are included in Figure 7a.

Appendix:

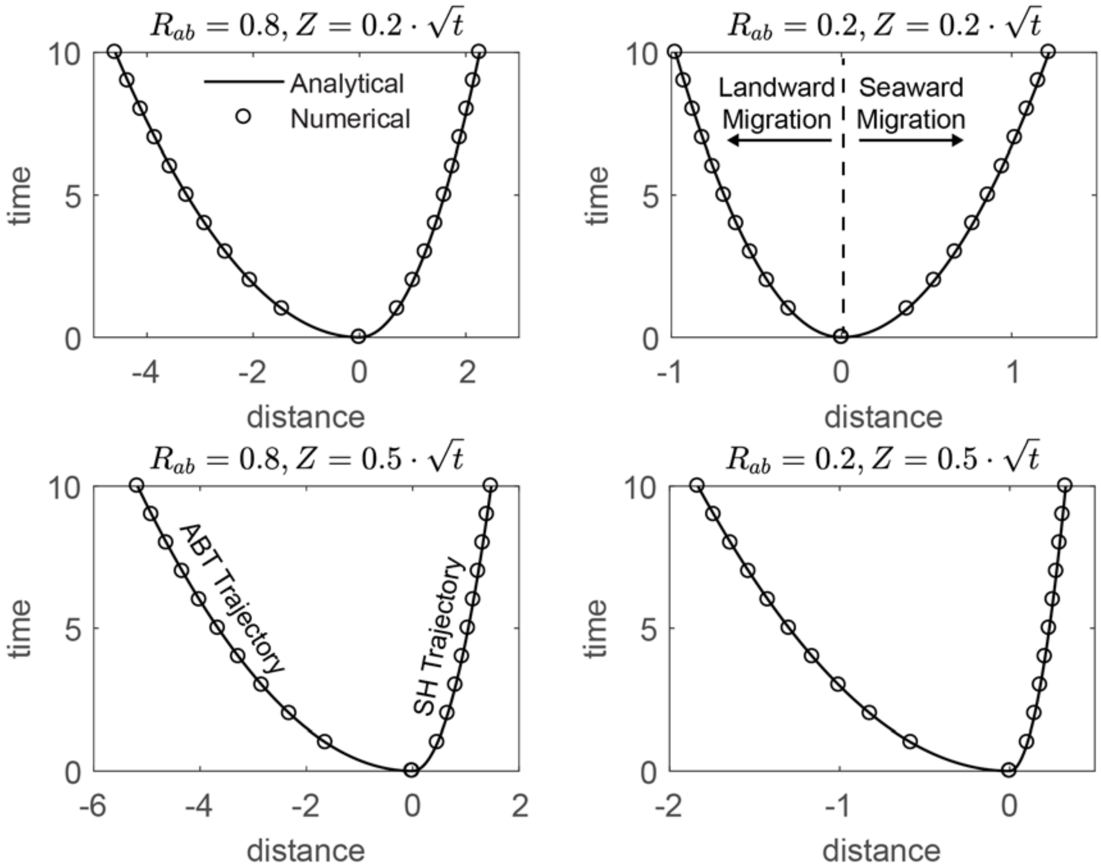

Figure A1. Comparison of analytical (solid lines) and numerical (circles) ABT and SH trajectories under square-root sea-level rise.

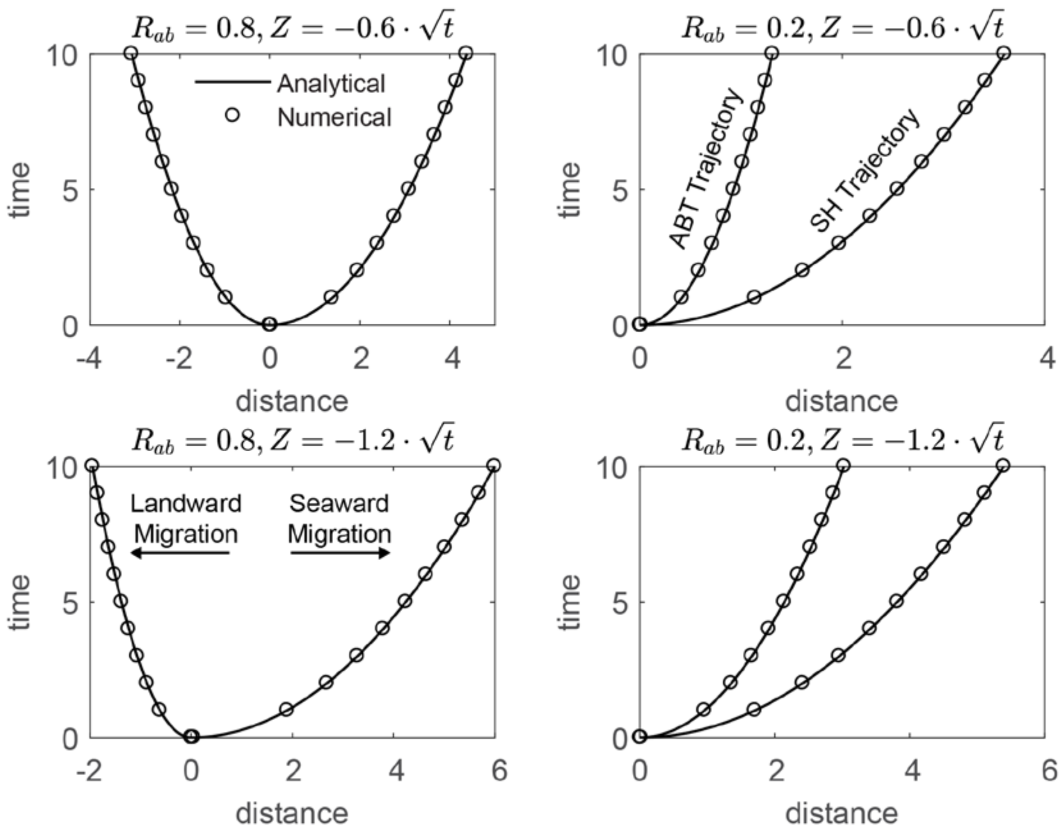

Figure A2. Comparison of analytical (solid lines) and numerical (circles) ABT and SH trajectories under square-root sea-level fall.

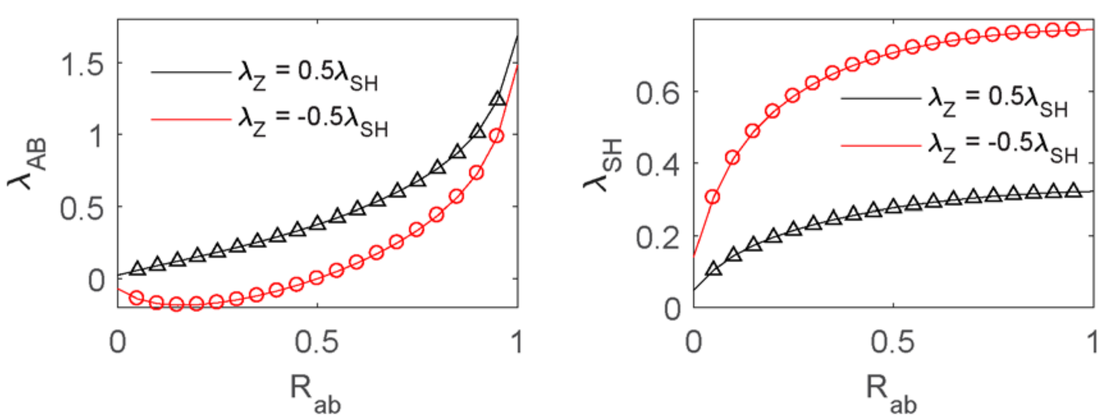

Figure A3. Comparison between analytical and numerical predictions of the moving boundary parameters λ_{sh} and λ_{ab} for the sea-level fall (circles) and sea-level rise (triangles) scenarios. The solid-line is the analytical solution and the symbols represent the enthalpy numerical solution described in section 4. We use $\Delta x = 0.01$ and $\Delta t = 5 \cdot 10^{-5}$.

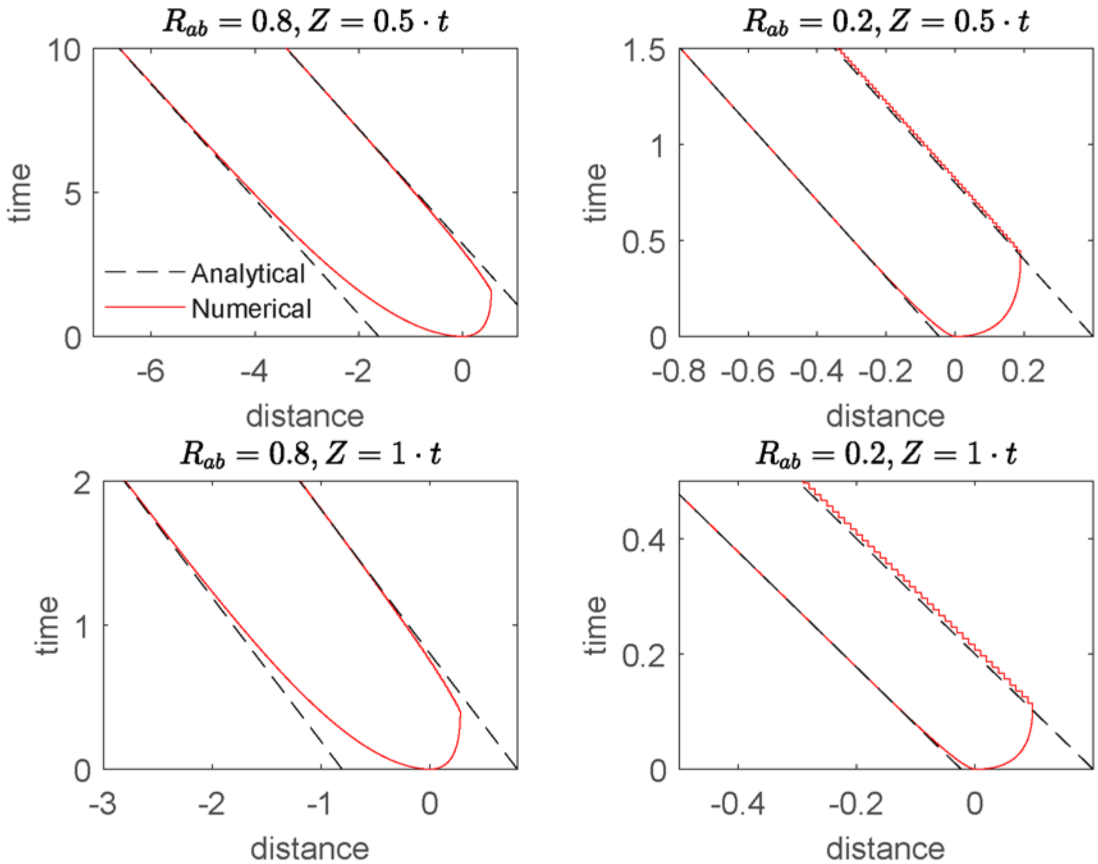

Figure A4. Comparison of analytical (dashed) and numerical (solid) ABT and SH trajectories under constant sea-level rise with $\Delta x = 0.01$ and $\Delta t = 5 \cdot 10^{-5}$.

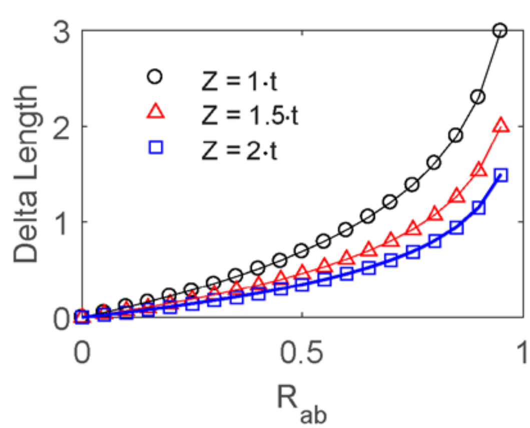

Figure A5. Comparison of analytical (solid lines) and numerical (symbols) delta length values (i.e., $s - r$) at steady state.